Barotropic and Baroclinic Annular Variability in the Southern Hemisphere

DAVID W. J. THOMPSON AND JONATHAN D. WOODWORTH

Department of Atmospheric Science, Colorado State University, Fort Collins, Colorado

(Manuscript received 20 June 2013, in final form 25 October 2013)

ABSTRACT

The leading patterns of large-scale climate variability in the Southern Hemisphere are examined in the context of extratropical kinetic energy. It is argued that variability in the Southern Hemisphere extratropical flow can be viewed in the context of two distinct and largely independent structures, both of which exhibit a high degree of annularity: 1) a barotropic structure that dominates the variance in the zonal-mean kinetic energy and 2) a baroclinic structure that dominates the variance in the eddy kinetic energy. The former structure corresponds to the southern annular mode (SAM) and has been extensively examined in the literature. The latter structure emerges as the leading principal component time series of eddy kinetic energy and has received seemingly little attention in previous work.

The two structures play very different roles in cycling energy through the extratropical troposphere. The SAM is associated primarily with variability in the meridional propagation of wave activity, has a surprisingly weak signature in the eddy fluxes of heat, and can be modeled as Gaussian red noise with an *e*-folding time scale of approximately 10 days. The baroclinic annular structure is associated primarily with variations in the amplitude of vertically propagating waves, has a very weak signature in the wave fluxes of momentum, and exhibits marked quasi periodicity on time scales of approximately 25–30 days. Implications for large-scale climate variability are discussed.

1. Introduction

Large-scale patterns of extratropical climate variability are typically identified through 1) correlation analyses between geographically separated points in the zonally varying circulation (i.e., so-called teleconnectivity) and/or 2) empirical orthogonal function (EOF) analysis. In both cases, the statistical analyses generally focus on the geopotential height, temperature, and/or zonal-wind fields. The purpose of this study is to investigate large-scale patterns of climate variability not from the perspective of the variance in the zonal wind or geopotential height fields per se, but rather from the perspective of the cycling of energy in the extratropical atmosphere.

The extratropical atmospheric energy cycle can be viewed in the context of reservoirs of zonal-mean and eddy available potential and kinetic energies, and the exchanges between these reservoirs (Fig. 1; Lorenz 1955; Vallis 2006). The zonal-mean available potential energy (APE) derives primarily from the meridional gradient in solar heating. The mean APE is converted to eddy APE through the meridional wave fluxes of heat (CP in Fig. 1), and the eddy APE is converted to eddy kinetic energy through the vertical wave fluxes of heat (CE in Fig. 1). In practice, the conversions given by CP and CE occur roughly simultaneously as warm air moves upward and poleward (and cool air moves downward and equatorward) within wave motions. The conversions between eddy and zonal-mean kinetic energy occur through the eddy fluxes of momentum (CK in Fig. 1). The Ferrel cell plays a relatively small role in cycling zonal-mean kinetic energy to zonal-mean available potential energy (CZ in Fig. 1).

Week-to-week variability in the cycling of energy in the midlatitude troposphere is due in large part to variations in the extratropical storm tracks and their associated fluxes of heat and momentum. This is particularly true in the Southern Hemisphere where the planetary wave amplitudes are relatively weak. Baroclinic waves play a crucial role in cycling eddy potential to eddy kinetic energy (CP and CE) during their growth stage and eddy to zonal-mean kinetic energy (CZ) during their decay stage (e.g., Simmons and Hoskins 1978; Vallis 2006).

Corresponding author address: David W. J. Thompson, Department of Atmospheric Science, Colorado State University, Campus Delivery 1782, Fort Collins, CO 80523.
E-mail: davet@atmos.colostate.edu

DOI: 10.1175/JAS-D-13-0185.1

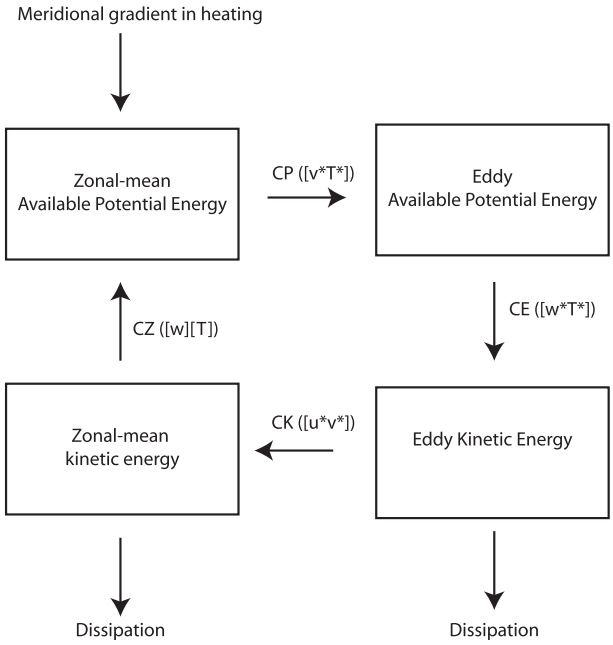

FIG. 1. Key processes in the midlatitude energy cycle (Lorenz 1955; Vallis 2006). Square brackets and asterisks denote the zonal-mean and eddy components of the flow, respectively.

Patterns of large-scale variability in the storm tracks are associated with variations in both the wave fluxes of heat and the eddy kinetic energy (e.g., Lau 1988; Wettstein and Wallace 2010). Patterns of large-scale variability in the midlatitude jet have been linked to fluctuations in many of the major reservoirs and conversion terms in the extratropical energy cycle, including the zonal-mean and eddy kinetic energy (e.g., Hartmann and Lo 1998) and the wave fluxes of both heat and momentum (e.g., Karoly 1990; Feldstein and Lee 1998; Hartmann and Lo 1998; Limpasuvan and Hartmann 2000).

In this study, we examine hemispheric-scale variability in the extratropical Southern Hemisphere (SH) from the perspective of atmospheric kinetic energy and the cycling of potential and kinetic energy by the extratropical wave fluxes of heat and momentum. The Northern Hemisphere will be considered in a companion study. The central argument is that large-scale variability in the SH extratropical flow can be viewed in the context of two unique structures, both of which exhibit a high degree of annularity: 1) a barotropic annular structure that dominates the variance of the zonal-mean kinetic energy and the eddy fluxes of momentum and 2) a baroclinic annular structure that dominates the variance in the eddy kinetic energy and the eddy fluxes of heat. The barotropic annular structure corresponds to the southern annular mode (SAM) and has been examined extensively in previous literature. The baroclinic annular structure plays a similarly important role in cycling energy through the extratropical atmosphere but has received seemingly little attention in previous work. Section 2 reviews the data and methods. Section 3 compares and contrasts the leading patterns of variability in SH extratropical zonal-mean and eddy kinetic energy. Key aspects of the results are discussed in section 4. Conclusions are given in section 5.

2. Data and methods

All results are based on the Interim European Centre for Medium-Range Weather Forecasts (ECMWF) Re-Analysis (ERA-Interim) dataset (Dee et al. 2011). The reanalysis output is available on a 1.25° × 1.25° mesh and at four-times-daily resolution from 1979 to the present. The results here are based on reanalysis output from 1979 to 2010. Anomalies are formed by subtracting the long-term mean seasonal cycle from the data at all grid points and vertical levels. All results are based on daily-mean data. Eddy fluxes are calculated at four-times-daily resolution and then averaged over 24 h to form daily means.

Throughout the study, square brackets denote the zonal mean and asterisks denote departures from the zonal mean. The zonal-mean kinetic energy (ZKE) is defined as $[u]^2/2$, the eddy kinetic energy (EKE) is defined as $[u^{*2} + v^{*2}]/2$, the eddy fluxes of momentum are defined as $[u^*v^*]$, and the eddy fluxes of heat are defined as $[v^*T^*]$.

The leading patterns of variability in various fields are identified through EOF–principal component (PC) analysis of anomalous daily-mean data. The leading PC of zonal-mean kinetic energy is defined as the leading PC of anomalous daily-mean $[u]^2/2$; the leading PC of zonal-mean eddy kinetic energy is defined as the leading PC of anomalous daily-mean $[u^{*2} + v^{*2}]/2$; the southern annular mode is defined as the leading PC of the anomalous daily-mean zonal-mean zonal wind $[u]$. In all cases, the PCs are computed over all levels and latitudes within the domain 1000–200 hPa and 20°–70°S. The data are weighted by the square root of the cosine of latitude and the mass represented by each vertical level in the ERA-Interim before calculating the PC time series.

The meridional and vertical components of the quasigeostrophic Eliassen–Palm (EP) flux are calculated as $F_\phi = -\rho_0 a \cos\phi [u^*v^*]$ and $F_z = f\rho_0 a \cos\phi ([v^*\theta^*]/[\theta]_z)$, respectively, where f denotes the Coriolis parameter, a is the radius of Earth, ϕ is the latitude, and ρ_0 is the air density as a function of height (e.g., Andrews et al. 1987). The EP flux is expressed here in units of kilograms per squared second; the divergence of the EP flux in units of meters per second per day.

Unless specifically noted, all PC time series are calculated for unfiltered daily-mean data. In some cases, correlations are shown for data that have been 10-day low-pass filtered to emphasize variability on time scales longer than those associated with individual baroclinic waves. In such cases, the data are filtered with a ninth-order Butterworth filter.

3. The leading patterns of variability in Southern Hemisphere kinetic energy

In this section, we will compare and contrast two patterns of variability that play very different roles in cycling energy in the SH extratropical circulation: the leading modes of variability in the SH zonal-mean and eddy kinetic energy. We begin our discussion with a review of the former.

a. The leading pattern of variability in SH zonal-mean kinetic energy (the SAM)

The leading PC time series of 1) the daily-mean, zonal-mean kinetic energy and 2) the daily-mean, zonal-mean zonal wind are correlated at a level of $r = 0.96$ (as noted in section 2, the PC time series are calculated over the domain 1000–200 hPa and 20°–70°S). The latter PC is commonly used to define fluctuations in the SAM, and thus the SAM corresponds to the leading mode of variability in the zonal-mean kinetic energy. The SAM has been extensively documented in the literature, but its distinction from the leading PC of eddy kinetic energy is a central theme in this study. For this reason, we will review key aspects of its signature here. By convention, the SAM index is standardized and positive values of the index correspond to anomalous westerly wind anomalies near 60°S, and vice versa.

The left columns in Figs. 2–4 review features of the SAM that are relevant for this study. Figure 2a shows the eddy momentum flux anomalies (shading; negative values denote southward momentum fluxes) and zonal-mean zonal-wind anomalies (contours) regressed onto the SAM index as a function of latitude and pressure. Figure 3a shows the regression coefficients at the 300-hPa level as a function of lag and latitude. As noted below, the momentum flux anomalies precede the peak in the SAM index by about 1–2 days (Lorenz and Hartmann 2001). For this reason, the eddy fluxes in the cross section presented in Fig. 2a are lagged by −1 day with respect to the SAM index.

As noted in previous work, the positive polarity of the SAM is characterized by 1) a meridional dipole in the zonal-mean zonal wind with centers of action located near 40°S and 60°S (Fig. 2a; e.g., Kidson 1988; Karoly 1990; Hartmann and Lo 1998; Thompson and Wallace 2000) and 2) a monopole in the eddy momentum fluxes centered near 50°S and about 300 hPa (Fig. 2a; e.g., Karoly 1990; Hartmann and Lo 1998; Limpasuvan and Hartmann 2000). The momentum flux anomalies precede and have a much shorter time scale than their counterparts in the zonal flow (Fig. 3a; Lorenz and Hartmann 2001). The lead–lag relationships between the momentum flux and zonal-flow anomalies are consistent with the linear, damped response of the circulation to mechanical forcing by the anomalous eddy fluxes of momentum (Lorenz and Hartmann 2001).

Figure 2c shows the signature of the SAM in the (Eulerian mean) mass streamfunction (contours; positive values denote clockwise motion) and temperature (shading). As also noted in previous work, the positive polarity of the SAM is marked by anomalously warm conditions at middle latitudes and cool conditions at both polar and subtropical latitudes (Figs. 2c; e.g., Thompson and Wallace 2000). The changes in the temperature field are consistent with mechanical forcing of the meridional circulation by the anomalous momentum fluxes aloft: regions of ascending motion are associated with adiabatic cooling, and vice versa (Fig. 2c; Thompson and Wallace 2000).

Figure 2e reviews the vertical structure of the SAM in the zonal-mean eddy fluxes of heat (shading; negative values denote southward heat fluxes) and eddy kinetic energy (contours). The wave fluxes are again lagged with respect to the SAM index by −1 day. Figure 4a highlights the time evolution of the heat flux anomalies at 850 hPa (shading) superposed on the evolution of the momentum flux anomalies at 300 hPa (contours) reproduced from Fig. 3a.

The SAM has a remarkably weak signature in the eddy fluxes of heat (shading in Figs. 2e and 4a). The most notable feature is the anomalously poleward heat fluxes centered 70°S approximately from lags +3 to +10 days (Fig. 4a). As discussed further in section 4, the anomalously poleward heat fluxes at positive lag are consistent with the effects of the anomalous momentum fluxes aloft on both baroclinicity and wave generation at lower-tropospheric levels (Robinson 2000; Lorenz and Hartmann 2001). The SAM is also marked by banded eddy kinetic energy anomalies that are consistent with meridional vacillations in the midlatitude jet and its embedded eddy fluxes (Fig. 2e; Hartmann and Lo 1998). As demonstrated below, the eddy heat flux and eddy kinetic energy anomalies associated with the SAM explain very small fractions of the total variance in their respective fields.

Figures 5b and 5d summarize the variances explained by the SAM in the eddy fluxes of heat and momentum (top) and the zonal-mean and eddy kinetic energy (bottom) as a function of latitude. The solid lines in

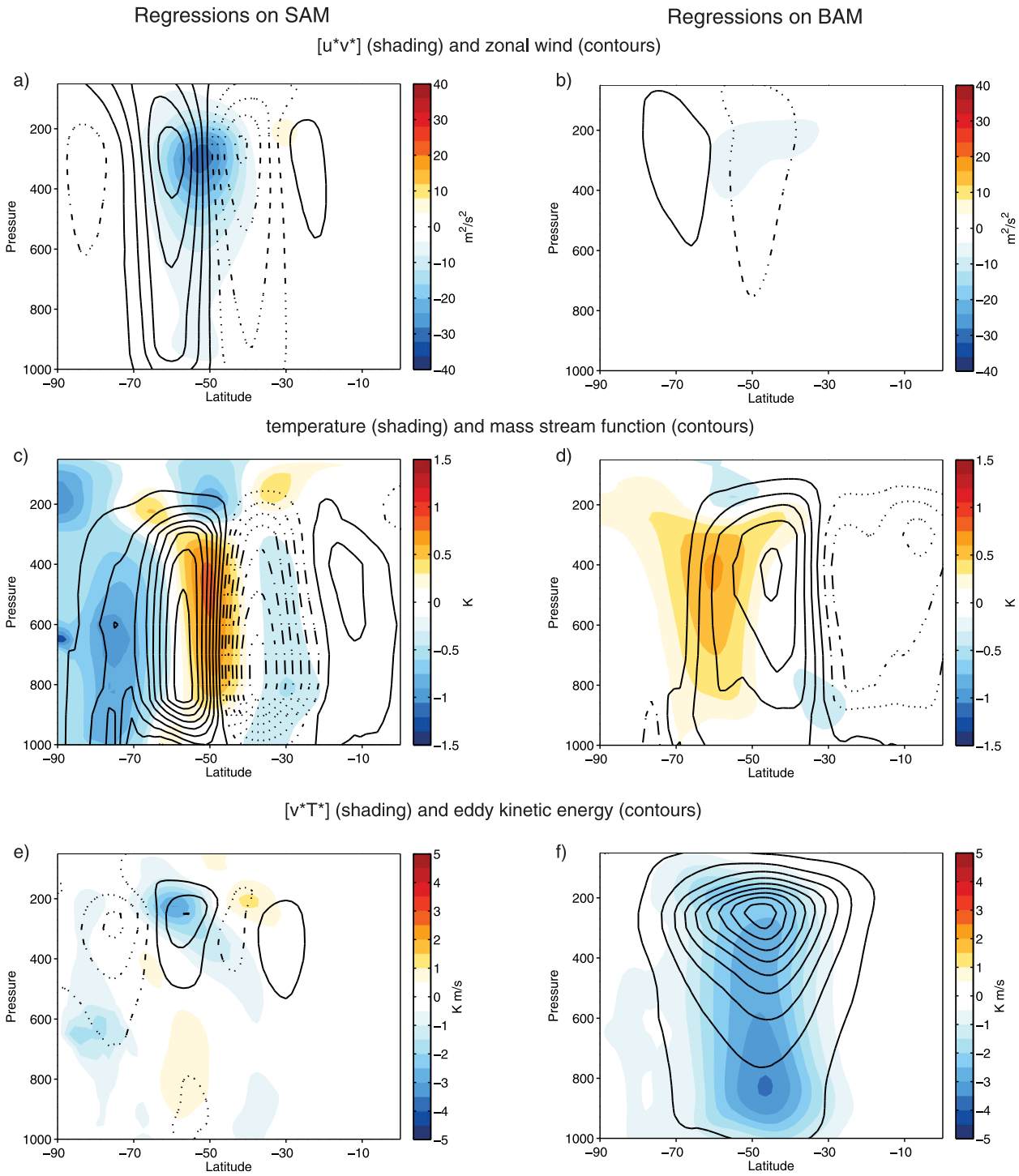

FIG. 2. Vertical structure of the SAM and BAM. Latitude–height regressions are based on standardized values of the (left) SAM and (right) BAM indices for the fields indicated (contours and shading are defined in panel titles). The SAM index is defined as the leading PC time series of the SH zonal-mean zonal wind. The BAM index is defined as the leading PC of the SH eddy kinetic energy. Results are based on zonal-mean, daily-mean data. Regression coefficients are based on contemporaneous values of the data, except in the cases of $[u^*v^*]$ and $[v^*T^*]$, in which the fluxes lead the SAM and BAM indices by 1 day. Contours are (a),(b) $-0.5, 0.5, 1.5, \ldots$ m s^{-1}; (c),(d) $-0.5, 0.5, 1.5, \ldots \times 10^9$ kg s^{-1}; and (e),(f) $-3, 3, 9, \ldots$ m^2 s^{-2}.

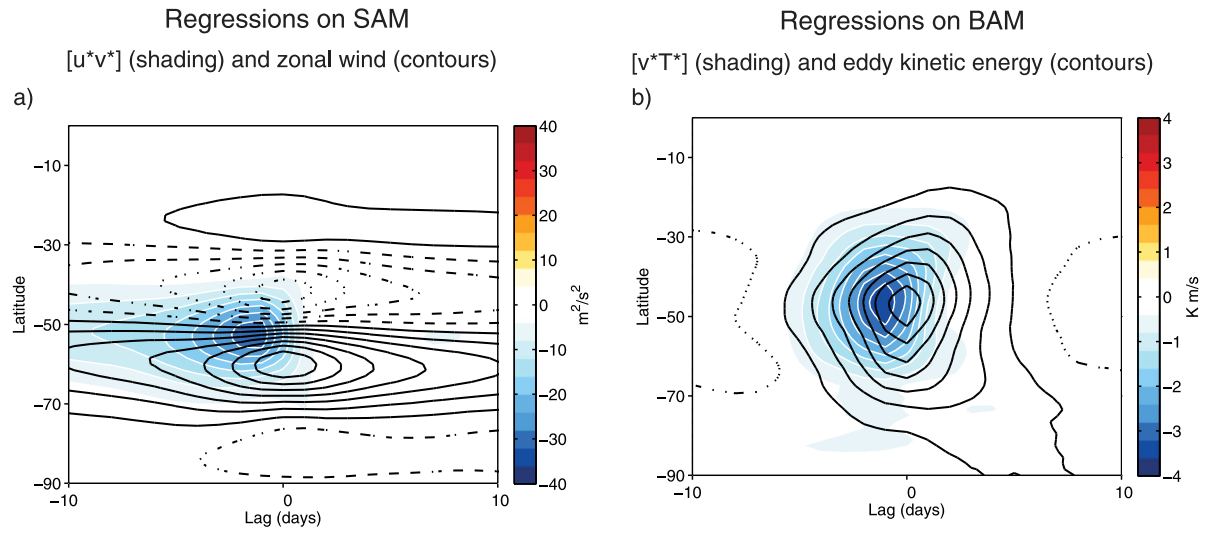

FIG. 3. Latitude–lag structure of the SAM and BAM in kinetic energy. Lead–lag regressions are based on standardized values of (a) the SAM index and (b) the leading PC of eddy kinetic energy (BAM) for the fields indicated (contours and shading are defined in panel titles). The momentum fluxes, zonal wind, and eddy kinetic energy are shown at 300 hPa. The heat fluxes are shown at 850 hPa. Negative lags denote the field leading the base index and vice versa. Results are based on zonal-mean, daily-mean data. Contours are shown at (a) $-0.35, 0.35, 1.05, \ldots$ m s^{-1} and (b) $-3.5, 3.5, 10.5, \ldots$ m^2 s^{-2}.

Fig. 6 summarize the variances explained by the SAM in the hemispherically integrated eddy kinetic energy (Fig. 6a) and eddy fluxes of heat (Fig. 6b) as a function of vertical level. The results are shown for 10-day low-pass-filtered versions of the data to highlight covariability on time scales longer than those associated with a typical baroclinic wave. The SAM explains more than 20% of the variance in the vertically integrated wave fluxes of momentum at middle latitudes, but almost none of the variance in the wave fluxes of heat, particularly at middle latitudes (Fig. 5a). Likewise, the SAM explains more than 80% of the variance in the zonal-mean zonal wind near 60° and 40°S (i.e., on the flanks of the climatological-mean jet) but only a small fraction of the variance in the eddy kinetic energy at all latitudes (Fig. 5c). The SAM explains a negligible fraction of the hemispheric mean in both the eddy kinetic energy and wave fluxes of heat (Figs. 6a and 6b).

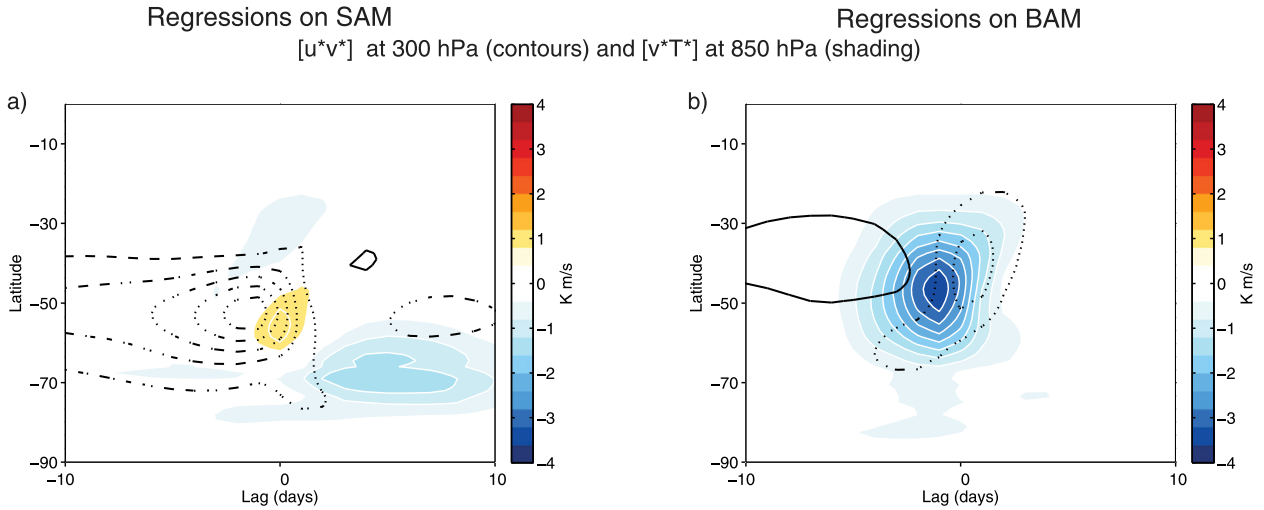

FIG. 4. Latitude–lag structure of the SAM and BAM in the eddy fluxes of heat and momentum. Lead–lag regressions are based on (a) standardized values of the SAM index and (b) the leading PC of eddy kinetic energy (BAM) for the fields indicated (contours and shading are defined in panel titles). Negative lags denote the field leading the base index and vice versa. Results are based on zonal-mean, daily-mean data. Contours are shown at $-3, 3, 9, \ldots$ m^2 s^{-2}.

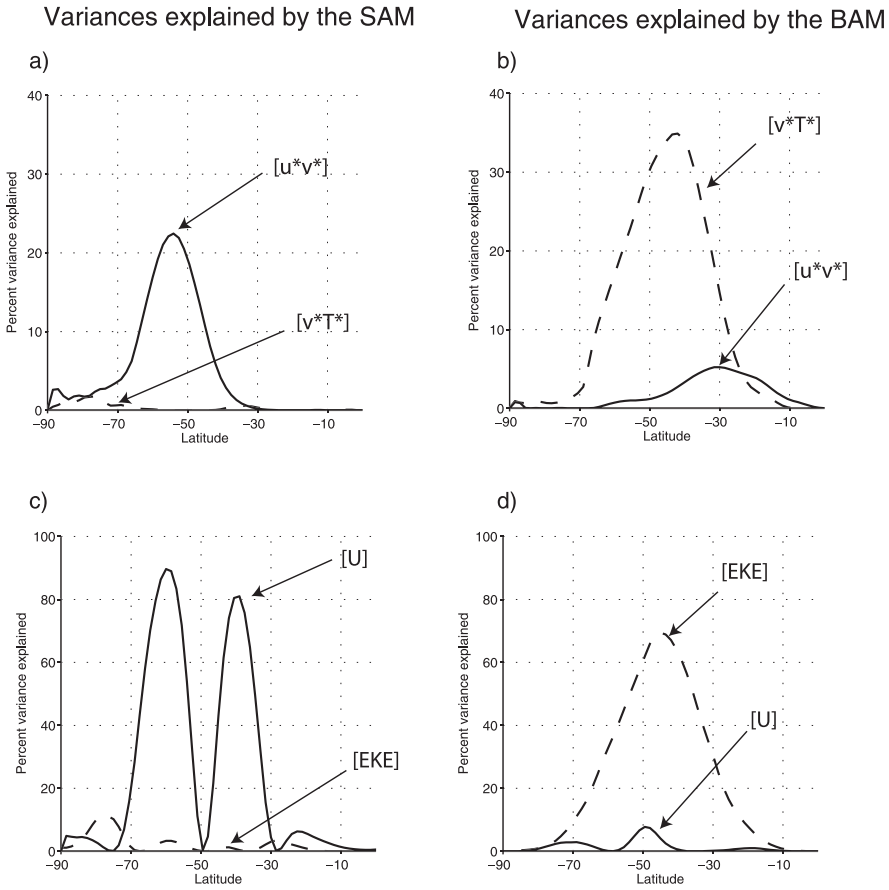

FIG. 5. Percentage variance explained by the (a),(c) SAM and (b),(d) BAM indices in vertically averaged data. The data are 10-day low-pass filtered to emphasize covariability on time scales longer than those associated with a typical baroclinic wave (the fluxes are formed from four-times-daily data before they are low-pass filtered). The fields are vertically averaged between 950 and 250 hPa.

The results shown above thus confirm and reproduce previous work but highlight a fundamental aspect of the SAM that has not been fully appreciated in the literature: the SAM has a pronounced signature in the wave fluxes of momentum and zonal-mean kinetic energy, but a very weak signature in the eddy fluxes of heat and eddy kinetic energy. The structure that dominates the latter fields will be investigated below.

b. The leading pattern of variability in SH eddy kinetic energy

What pattern of variability explains the predominant fraction of the variance in the SH extratropical eddy fluxes of heat and eddy kinetic energy? The results shown in the right panels in Figs. 2–4 are analogous to those shown in the left panels but are based on standardized values of the leading PC of the Southern Hemisphere eddy kinetic energy. The right panels in Figs. 2 and 4 show the same fields as the left panels; the right panel in Fig. 3 shows the time evolution of the eddy fluxes of heat and eddy kinetic energy.

The leading PC of the Southern Hemisphere eddy kinetic energy is calculated for data at all levels and latitudes between 20° and 70°S and 1000 and 200 hPa. It explains 34% of the daily-mean variance in SH zonal-mean extratropical eddy kinetic energy, is reproducible during the SH cold and warm seasons, and is well separated from its second PC according to the criterion in North et al. (1982; Table 2). The leading PC of eddy kinetic energy is also, to first order, linearly independent of the SAM: the correlations with the SAM index are 1) less than $r = 0.1$ in daily data for all lags between −30 and 30 days and 2) $r = 0.06$ for time series that have been 10-day low-pass filtered (Table 1). As noted below, the leading PC of SH eddy kinetic energy exhibits a high degree of annularity but is associated primarily with baroclinic (rather than barotropic) processes. To contrast the leading PC of SH of eddy kinetic energy from the

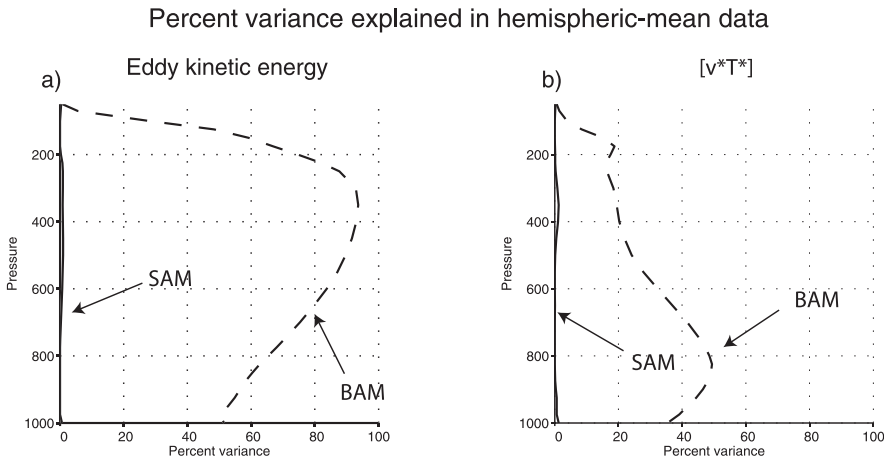

FIG. 6. Percentage variance explained in (a) hemispherically averaged eddy kinetic energy and (b) the wave fluxes of heat by the SAM and BAM indices. The data are 10-day low-pass filtered to emphasize covariability on time scales longer than those associated with a typical baroclinic wave (the fluxes are formed from four-times-daily data before they are low-pass filtered). The fields are averaged between 20° and 70°S.

SAM, we will herein refer to it as a SH baroclinic annular mode (BAM).

The SAM and BAM have strikingly different signatures in the extratropical circulation. The BAM index time series is associated with broad monopoles in both the eddy kinetic energy and eddy fluxes of heat that span much of the SH extratropics (Fig. 2f; by definition, positive values of the BAM index correspond to positive anomalies in SH eddy kinetic energy, and vice versa). The eddy kinetic anomalies associated with the BAM peak immediately above (Fig. 2f) and several days after (Fig. 3b) the eddy heat flux anomalies. They are thus consistent with the generation of eddy kinetic energy by anomalous wave growth in the lowermost troposphere (wave generation near the surface is proportional to the vertical derivative of the heat fluxes at the lower boundary).

The SAM and BAM index time series also have very different signatures in the zonal-mean temperature and zonal-wind fields. The positive polarity of the BAM is marked by warm temperature anomalies throughout the mid- to high-latitude troposphere (Fig. 2d) but by relatively weak anomalies in both the zonal-mean zonal wind and the eddy fluxes of momentum (Fig. 2b). The anomalous (Eulerian mean) mass streamfunction (Fig. 2d) is consistent with rising motion in regions of heating by the eddies (i.e., the anomalous heat fluxes converge poleward of about 50°S). The anomalous upper-tropospheric easterlies centered near 50°S (Fig. 2b) are consistent with the Coriolis torque acting on the anomalous (Eulerian mean) equatorward motion there. As discussed further in section 4, the most notable momentum flux anomalies associated with the BAM are found between 30° and 50°S several days after the peak in wave fluxes of heat (Fig. 4b).

Unlike the SAM, the BAM explains a notable fraction of the variance in the 10-day low-pass wave fluxes of heat and eddy kinetic energy at middle latitudes (dashed lines in Figs. 5b and 5d). It also explains a very small fraction of the variance in the wave fluxes of momentum and the zonal-mean zonal wind throughout the SH (solid lines in Figs. 5b and 5d). The BAM explains up to about 50% of the variance in the hemispherically integrated eddy fluxes of heat in the lower troposphere (Fig. 6b) and up to about 90% of the variance in the hemispherically integrated eddy kinetic energy in the upper troposphere (Fig. 6a). The SH mean eddy kinetic energy at 300 hPa is correlated with the BAM index at a level of $r \approx 0.95$.

Note that the BAM is not simply a proxy for higher-order PCs of the zonal-mean-wind field. For example, the second PC of the zonal-wind field is characterized by variations in the amplitude of the extratropical jet (see also Lorenz and Hartmann 2001). The second PC of the zonal-mean zonal wind explains a notable fraction of the 10-day low-pass variance in the wave fluxes of momentum

TABLE 1. Correlations between the leading PCs of the zonal-mean fields indicated. The PCs are calculated for daily-mean versions of the data. Correlations are computed between 10-day low-pass-filtered versions of the resulting PC time series. Boldface font indicates results that are significant at the 95% confidence level based on a two-tailed test of the t statistic.

	PC 1 EKE	PC 1 ZKE	PC 1 U (SAM)
PC 1 EKE	**1**	0.05	0.06
PC 1 ZKE	0.05	**1**	**0.97**

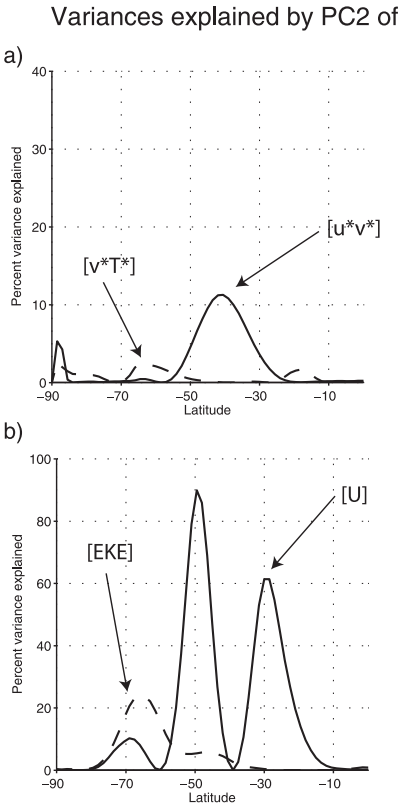

FIG. 7. As in Fig. 5 (left), except correlations are based on the second PC of the Southern Hemisphere zonal-mean zonal wind.

in midlatitudes near 40°S and in the zonal-mean zonal wind near 50° and 30°S (solid lines in Figs. 7a and 7b), but it explains a relatively small fraction of the variance in the eddy fluxes of heat and eddy kinetic energy throughout most of the SH midlatitudes (dashed lines in Figs. 7a and 7b). The peak in eddy kinetic energy along the perimeter of Antarctica near 70° does not project onto the signature of the BAM in eddy kinetic energy.

4. Discussion

a. *The contrasting roles of the BAM and SAM in the wave fluxes of heat and momentum*

The eddy fluxes of heat and momentum are intrinsically linked through wave propagation in the atmosphere. The wave fluxes of heat are proportional to vertical wave propagation; the wave fluxes of momentum are proportional to meridional wave propagation. Wave generation in the lower troposphere provides a source for meridional wave propagation aloft (e.g., Simmons and Hoskins 1978; Randel and Stanford 1985); meridional wave propagation aloft influences lower-tropospheric baroclinicity and thus the conditions for wave generation near the surface (e.g., Robinson 2000). Linkages between the eddy fluxes of heat and momentum are believed play a role in the feedbacks that lead to internal atmospheric variability (e.g., Robinson 2000; Lorenz and Hartmann 2001). Taken together, the wave fluxes of heat and momentum describe the net wave forcing on the extratropical flow (e.g., Andrews and McIntyre 1976).

The results shown in the previous section highlight a notable level of decoupling between the wave fluxes of heat and momentum associated with the leading modes of extratropical kinetic energy. The BAM is associated primarily with variability in the wave fluxes of heat and has only a modest signature in the wave fluxes of momentum; the SAM is associated primarily with variations in the wave fluxes of momentum and has a very weak signature in the wave fluxes of heat. From the perspective of the baroclinic wave life cycle, the BAM describes variability in the amplitude of developing baroclinic waves, whereas the SAM describes variability in the meridional propagation of the wave activity aloft.

The contrasting signatures of the SAM and BAM in the wave fluxes of heat and momentum are further elucidated in the EP flux cross sections shown in Fig. 8. Figures 8a and 8b show the EP fluxes and their divergences regressed on the SAM and BAM indices and then averaged over the ''onset'' stages of both patterns of variability; Figs. 8c and 8d show the regressions averaged over the ''decay'' stages. The onset stage is defined as the 3-day period before peak amplitude in the SAM and BAM; the decay stage as the 3-day period after peak amplitude in both patterns of variability.

As reviewed in section 3, the onset stage of the SAM is associated with large anomalies in the meridional flux of wave activity and thus of zonal momentum (horizontal arrows in Fig. 8a). The anomalous wave fluxes of momentum drive the SAM-related zonal-wind anomalies (Lorenz and Hartmann 2001), and they also drive changes in the meridional circulation that project onto the low-level baroclinicity (Robinson 2000). The baroclinicity anomalies, in turn, are associated with weak changes in the wave fluxes of heat that peak during the decay stage of the SAM (vertical arrows near the surface in Fig. 8c; Lorenz and Hartmann 2001). Hence, the primary heat flux anomalies associated with the SAM can be viewed as a response to the changes in the wave fluxes of momentum aloft.

In contrast, the onset stage of the BAM is associated primarily with changes in the wave fluxes of heat (Fig. 8b). The heat fluxes reflect the upward radiation of wave activity from the lower troposphere, and the preponderance of the flux is dissipated immediately above the lower-tropospheric source (Fig. 8b). During the decay stage of the BAM, a component of the wave flux appears

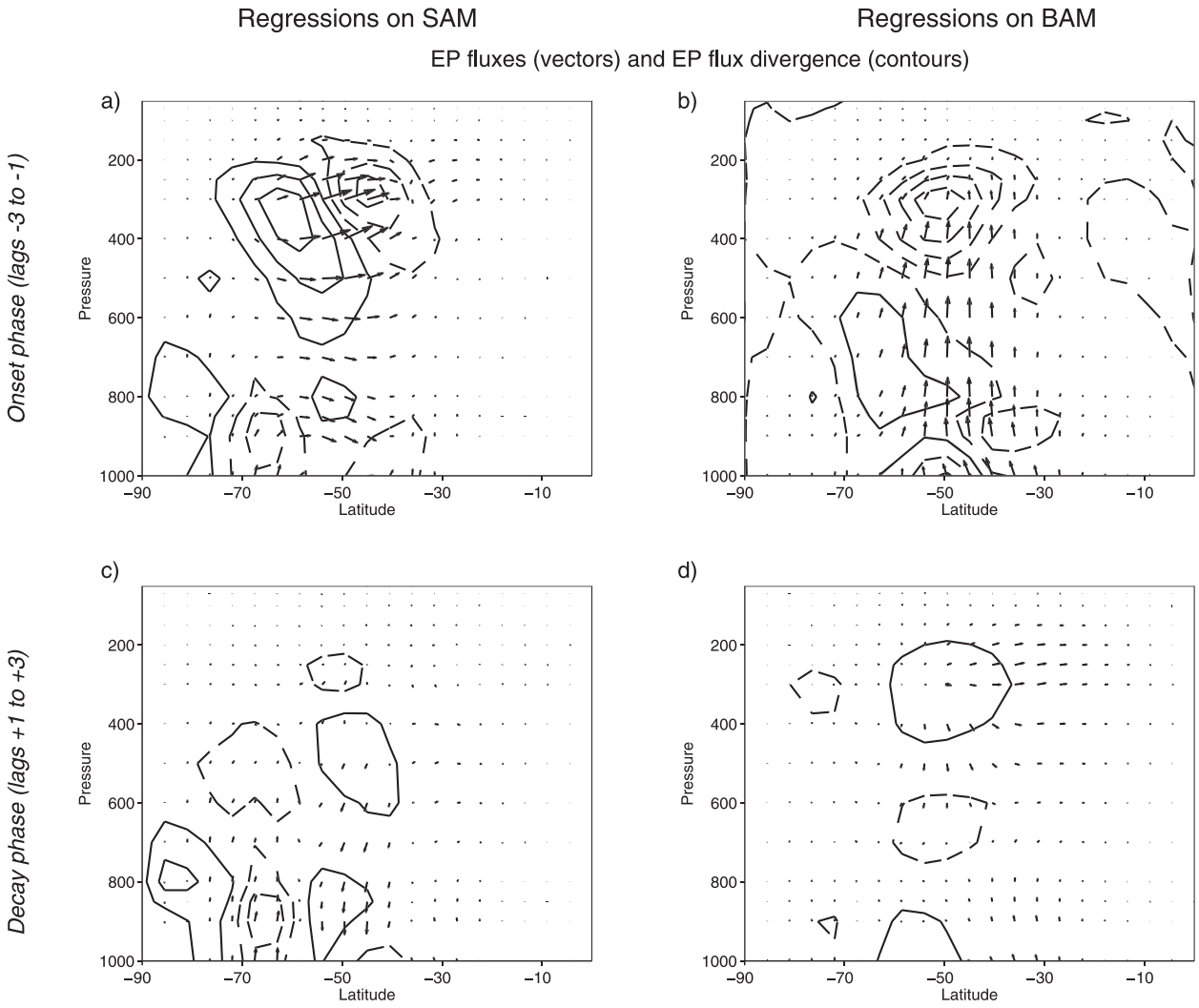

FIG. 8. Vertical structure of the SAM and BAM in the EP flux (vectors) and its divergence (contours). Latitude–height regressions are based on standardized values of the (a),(c) SAM and (b),(d) BAM indices for the fields indicated. (top) Regressions averaged over the onset phase of the SAM and BAM (defined as lags −3 to −1 days); (bottom) regressions averaged over the decay phase of the SAM and BAM (defined as lags +1 to +3 days). Contours are shown at −0.5, 0.5, 1.5, ... $\mathrm{m\,s^{-1}\,day^{-1}}$. The longest vector is approximately $5 \times 10^7\,\mathrm{kg\,s^{-2}}$ (horizontal) and $2 \times 10^5\,\mathrm{kg\,s^{-2}}$ (vertical).

to propagate equatorward, consistent with the barotropic dispersion of wave activity away from the high-latitude source (Fig. 8d). Hence, the primary momentum flux anomalies associated with the BAM can be viewed as a response to the changes in the wave fluxes of heat in the lower troposphere.

The amplitudes of the upper-tropospheric wave forcings associated with the BAM are comparable to those associated with the SAM (contours in Figs. 8a and 8b). Interestingly, the zonal-wind anomalies associated with the BAM are only about 25% as large as those associated with the SAM (e.g., Figs. 2a and 2b). The relatively weak signature of the BAM in the zonal-mean flow is consistent with the observation that the acceleration of the zonal flow is much larger for a given change in the horizontal EP flux divergence than it is for a similar change in vertical EP flux divergence (e.g., Pfeffer 1992).

The notable amount of decoupling between the vertical and meridional fluxes of wave activity associated with the SAM and BAM is also explicit in PC analyses based on the wave fluxes of momentum and heat. The leading PC of the eddy momentum fluxes explains a large fraction of the variance in the tropospherically integrated wave fluxes of momentum (Table 2; solid line in Fig. 9a) but a relatively small fraction of the variance in the tropospherically integrated wave fluxes of heat (dashed line in Fig. 9a). The leading PC of the SH eddy heat fluxes

TABLE 2. Variances explained (%) by the leading PCs of the zonal-mean fields indicated. The PCs are calculated for daily-mean versions of the data (the eddy fluxes are calculated at four-times-daily resolution and then averaged to form daily means). All leading PCs are well separated from the second PC as per the criterion outlined in North et al. (1982).

	[EKE]	[ZKE]	[U]	[u^*v^*]	[v^*T^*]
Variance explained by PC1 (PC2)	34 (19)	39 (27)	42 (22)	47 (22)	29 (16)

explains a large fraction of the variance in the tropospherically integrated wave fluxes of heat (Table 2; dashed line in Fig. 9b) but is only weakly correlated with the tropospherically integrated wave fluxes of momentum (solid line in Fig. 9b).

b. *Signatures in the zonally varying circulation*

The SAM and BAM both exhibit a high degree of annularity in the zonally varying circulation. Figures 10a and 10b show composite differences in the upper-tropospheric zonal wind and eddy kinetic energy between high- and low-index days in the SAM (Fig. 10a) and BAM (Fig. 10b) index time series. High- and low-index days are defined as days on which the respective index time series exceeds one standard deviation in absolute value. The SAM exhibits notable zonal asymmetries in the zonal-wind field (e.g., Cordron 2007; Barnes and Hartmann 2010) but is nevertheless dominated by its zonally symmetric component. The signature of the BAM in eddy kinetic energy bears strong resemblance to the leading EOF of the Southern Hemisphere high-pass-filtered 300-hPa meridional wind variance (Wettstein and Wallace 2010; cf. Fig. 1). It peaks in a region extending eastward from the South Atlantic to Australia, but clearly derives from all sectors of the hemisphere. The differences between the amplitudes of the eddy kinetic energy and zonal-flow anomalies associated with the SAM and BAM are striking throughout middle and high latitudes.

The robustness of the zonally symmetric signature of the BAM is supported by principal component analysis of the longitudinally varying eddy kinetic energy field. Figure 11a shows the correlations between 1) time series of the zonal-mean 300-hPa eddy kinetic energy and 2) the leading PC time series of the longitudinally varying 300-hPa eddy kinetic energy. The zonal mean and PC time series are calculated as a function of latitude, and the data are 10-day low-pass filtered to emphasize covariability on time scales longer than those associated with individual baroclinic waves. For example, the correlation coefficient at 65°S corresponds to the correlation between the time series of 1) the 10-day low-pass, zonal-mean eddy kinetic energy at 65°S and 2) the leading PC time series of the 10-day low-pass, longitudinally varying eddy kinetic energy at 65°S. The results thus provide a quantitative measure of the ''annularity'' of the leading PCs of the eddy kinetic field as a function of latitude.

As evidenced in Fig. 11a, the leading PCs of the longitudinally varying eddy kinetic field explain a large fraction of the variance in the zonal-mean circulation throughout the Southern Hemisphere, with correlation coefficients exceeding $r = 0.9$ at middle latitudes. The leading PCs of the longitudinally varying 300-hPa eddy kinetic energy

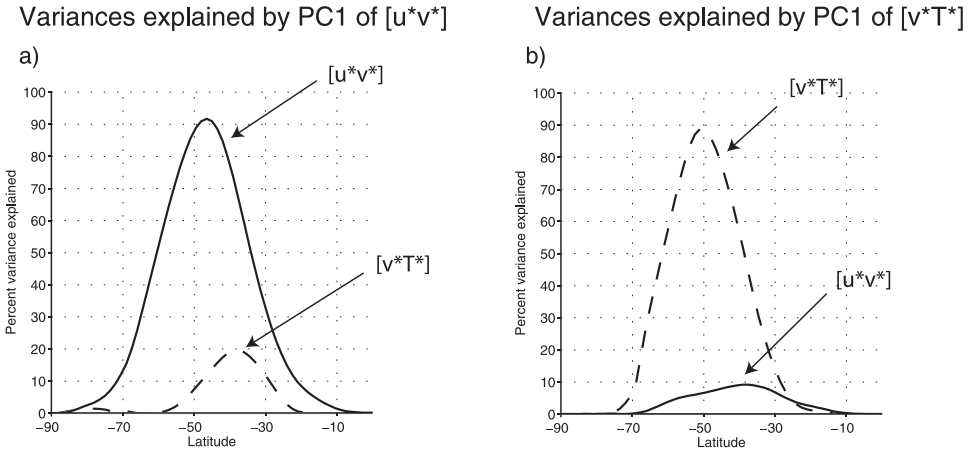

FIG. 9. Percentage variance explained in the fields indicated by the leading PCs of the eddy fluxes of (a) momentum and (b) heat. Results are based on wave fluxes that have been vertically averaged between 950 and 250 hPa. The data are 10-day low-pass filtered to emphasize covariability on time scales longer than those associated with a typical baroclinic wave (the fluxes are formed from four-times-daily data before they are low-pass filtered).

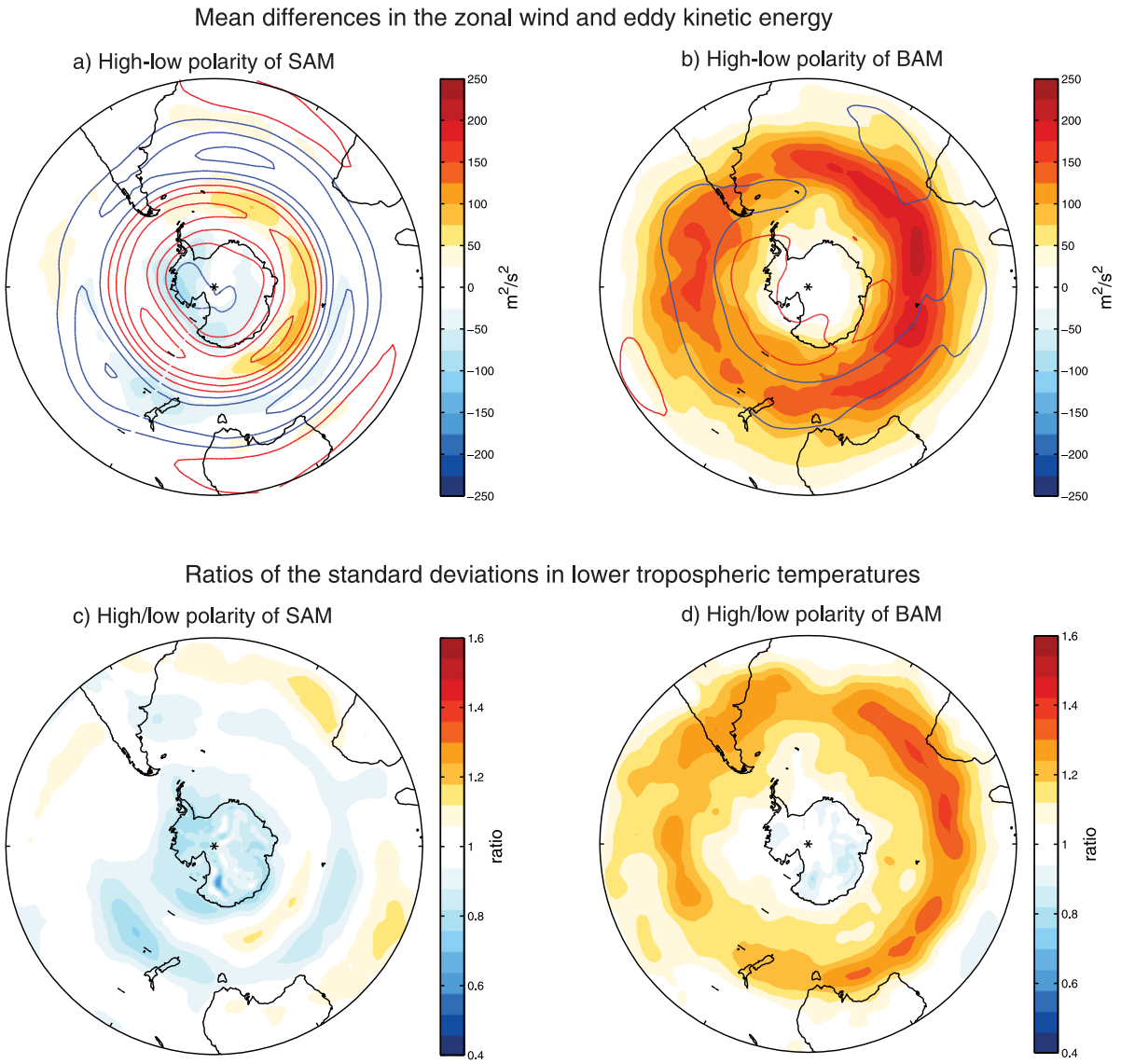

FIG. 10. Horizontal structures of the BAM and SAM. (top) Composite mean differences in the zonal wind at 250 hPa (contours) and eddy kinetic energy at 300 hPa (shading) between days that fall under the high- and low-index polarities of the (a) SAM and (b) BAM indices. Contours of the zonal wind are drawn at $-2.5, 2.5, 7.5, \ldots$ m s^{-1} (blue indicates negative values). (bottom) Ratios of the standard deviation of temperature at 700 hPa between days that fall under the high- and low-index polarities of the (c) SAM and (d) BAM indices.

field are distinct from their associated second PCs at all latitudes poleward of about 30°S, according to the criterion given in North et al. (1982) (Fig. 11b).

The distinctions between the SAM and BAM also extend to their signatures in near-surface climate. To first order, the surface climate impacts of the SAM reflect changes in the mean climate (e.g., local increases or decreases in temperature and precipitation). In contrast, the surface climate impacts of BAM reflect changes in the variance of surface climate. Figures 10c and 10d show the ratios in the variance of daily-mean 700-hPa temperatures between high and low index days in the SAM (Fig. 10c) and BAM (Fig. 10d) indices. In general, the positive polarity of the SAM is marked by relatively weak changes in the day-to-day variability of lower-tropospheric temperature. In contrast, the positive polarity of BAM is marked by notable increases in temperature variance throughout much of the SH middle latitudes. The peak ratios are found in a zonally elongated band that stretches from the south of Africa to the south of Australia and are coincident with a region of relatively large near-surface baroclinicity (not shown).

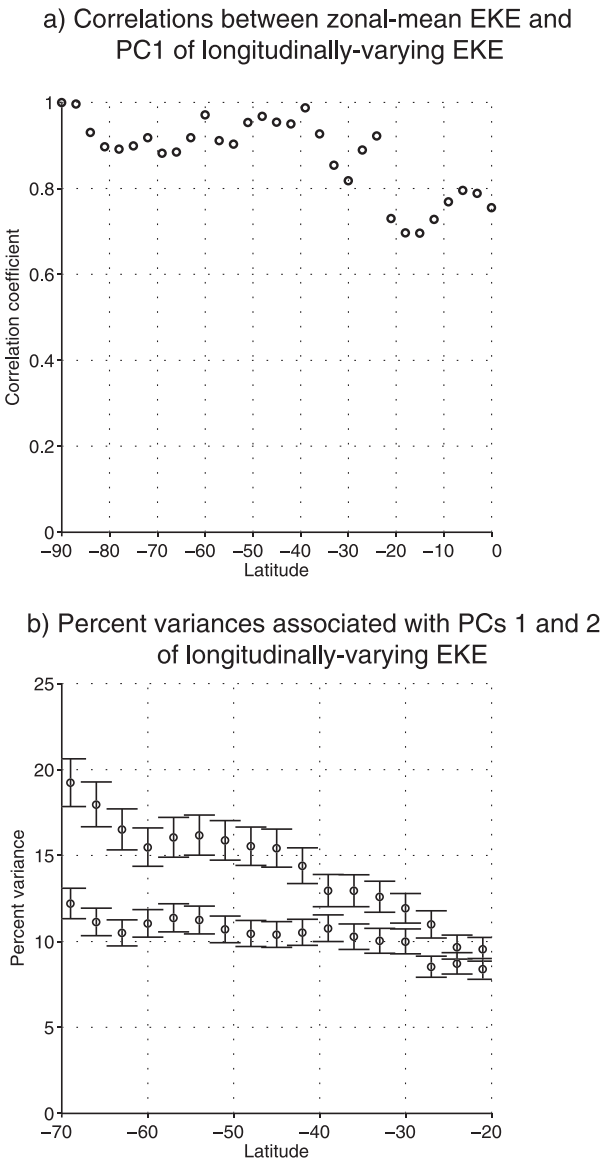

FIG. 11. Assessing the annularity of the BAM in the eddy kinetic energy at 300 hPa. (a) Correlations between zonal-mean EKE and the leading PCs of longitudinally varying EKE. The zonal-mean EKE and the PCs of the longitudinally varying EKE are calculated as a function of latitude. (b) Variances explained by the first and second PCs of longitudinally varying EKE, calculated as a function of latitude. Error bars are derived from the significance test described in North et al. (1982). The data are 10-day low-pass filtered to emphasize covariability on time scales longer than those associated with a typical baroclinic wave (the eddy time series are formed from four-times-daily data before they are low-pass filtered).

c. *Quasi periodicity in the baroclinic annular mode*

The distinctions between the SAM and BAM also extend to the time scales of their variations. Figures 12a and 12b show the power spectra of the SAM and BAM index time series. The results are found by

1) Calculating the spectra for subsets of the time series that are 500 days in length. A Hanning window is applied to each subset, and the overlap between adjacent subsets is 250 days.
2) Averaging the power spectra over all subsets and then applying a three-point running mean to the resulting mean power spectra. The mean spectrum for each time series has approximately 140 degrees of freedom per spectral estimate.

The power spectrum of the SAM (Fig. 12a) is red with an *e*-folding time scale of about 10 days (Hartmann and Lo 1998; Lorenz and Hartmann 2001). The shape of the spectrum is consistent with the damped response of the zonal-wind field to approximately white-noise forcing by the eddy fluxes of momentum (Lorenz and Hartmann 2001). In contrast, the power spectrum of the BAM (Fig. 12b) is red at frequencies higher than about 0.05 cpd (periods shorter than about 20 days) but exhibits a notable dropoff in power at frequencies lower than about 0.04 cpd. Hence, the power spectrum of BAM is marked by pronounced quasi periodicity that peaks on a time scale of about 20–30 days.

The quasi periodicity in the BAM index is extremely robust. It is reproducible in subsets of the data (not shown), during both the warm and cold seasons (not shown) and exceeds the 95% confidence level based on tests of 1) the *F* statistic applied to the power spectrum (assuming a red-noise fit to the data) and 2) the *t* statistic applied to the autocorrelation function (assuming the appropriate number of degrees of freedom). A similar peak in the SH circulation was detected in 1 year of balloon measurements taken during the Eole experiment (Webster and Keller 1974, 1975) and in 3 years of gridded geopotential height data (Randel and Stanford 1985). The result in Fig. 12b provides support for a robust peak in the primary pattern of variability in SH eddy kinetic energy based on more than 30 years of reanalysis data.

The implications of and physical process that drives the observed quasi periodicity in the BAM are investigated in a companion study (Thompson and Barnes 2014).

5. Concluding remarks

Hemispheric-scale variability in Southern Hemisphere extratropical kinetic energy is dominated by two largely independent structures: the leading PC of the zonal-mean kinetic energy (the SAM) and the leading PC of the eddy kinetic energy (the BAM). The two structures play markedly different roles in cycling energy through the extratropical circulation. The SAM accounts for the preponderance of the variance in the eddy fluxes of momentum and the zonal-mean kinetic energy but a very

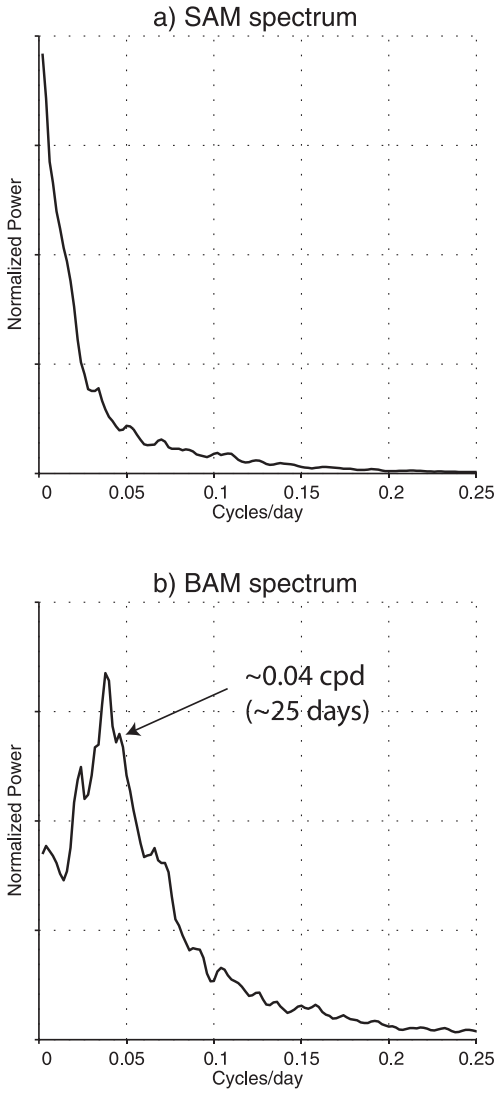

FIG. 12. Power spectra of the SAM and BAM indices. See text for details of the calculations.

small fraction of the variance in the eddy fluxes of heat and the eddy kinetic energy. The BAM accounts for large fractions of the variance in both the wave fluxes of heat and eddy kinetic energy but very little of the variance in the wave fluxes of momentum and zonal-mean kinetic energy.

The SAM and BAM both exhibit a high degree of zonal symmetry in the extratropical zonal wind and eddy kinetic energy fields, respectively. Additionally, the leading patterns of variability in the longitudinally varying eddy kinetic energy field include a pronounced zonally symmetric component. Hence, not only the SAM but also the BAM may be viewed as an ''annular mode'': the SAM as a barotropic annular mode (i.e., an annular structure driven by barotropic processes) and the BAM as a baroclinic annular mode (i.e., an annular structure driven by baroclinic processes). From a synoptic point of view, the SAM describes variations in the meridional propagation of wave activity, whereas the BAM describes variations in the amplitude of developing baroclinic waves. The notable level of decoupling between the wave fluxes of heat and momentum associated with the SAM and BAM suggests that variations in the amplitude and barotropic components of the storm track exhibit a high degree of independence.

The SAM is believed to owe its existence to enhanced power at low frequencies due to feedbacks between the momentum flux convergence aloft and the generation of wave activity near Earth's surface (Robinson 2000; Lorenz and Hartmann 2001). The results shown here suggest that the BAM owes its existence, not to enhanced power at low frequencies, but to enhanced power on a time scale of approximately 20–30 days. The quasi periodicity apparent in the BAM index is extremely robust and emerges during both the warm and cold seasons. The implications of and mechanisms that drive the observed periodicity in the BAM are explored in a companion study (Thompson and Barnes 2014).

We have performed similar analyses for the Northern Hemisphere circulation. The results for the NH are complicated by the effects of the stationary waves. But many of the primary results and conclusions derived for the zonal-mean SH circulation hold for both 1) the Northern Hemisphere zonal-mean circulation and 2) the North Atlantic and North Pacific storm-track regions considered separately. The leading PC time series of eddy kinetic energy calculated for the NH zonal-mean circulation, the North Atlantic sector, and the North Pacific sector are all marked by a monopole in eddy kinetic energy, account for large fractions of the domain-integrated variance in the wave fluxes of heat, and have only weak projections on the wave fluxes of momentum. Likewise, the attendant leading PC time series of NH zonal-mean kinetic energy account for large fractions of the domain-integrated variance in the wave fluxes of momentum but not of heat. The NH results will be presented in a companion paper.

Taken together, the SAM and BAM describe much of the variance in the cycling of energy in the extratropical SH atmosphere. The robustness of the BAM time series (Table 2), its pronounced role in the cycling of energy in the SH midlatitudes, and its unique time scale all suggest it may provide a useful framework for interpreting large-scale climate variability across a range of time scales, including the circulation response to climate change. Anthropogenic emissions of greenhouse gases are likely to perturb the tropospheric reservoirs of zonal-mean available potential energy and zonal-mean kinetic energy

through their projection on the meridional gradients in temperature. Climate change simulations driven by increasing greenhouse gases are marked not only by poleward shifts in the midlatitude jets reminiscent of the SAM (Kushner et al. 2001; Miller et al. 2006) but also by hemispheric-scale increases in extratropical eddy kinetic energy (Yin 2005) and the eddy fluxes of heat (O'Gorman 2010). To what extent the BAM projects onto the climate response to external forcing remains to be determined.

Acknowledgments. Thanks to Brian J. Hoskins, R. Alan Plumb, James A. Renwick, and John M. Wallace for helpful discussion of the results, three anonymous reviewers for constructive and insightful comments on the manuscript, and Ying Li and Kevin M. Grise for assistance with the data. DWJT and JDW were funded by the National Science Foundation Climate Dynamics program.

REFERENCES

Andrews, D. G., and M. E. McIntyre, 1976: Planetary waves in horizontal and vertical shear: The generalized Eliassen-Palm relation and the mean zonal acceleration. *J. Atmos. Sci.,* **33,** 2031–2048.

——, J. R. Holton, and C. B. Leovy, 1987: *Middle Atmosphere Dynamics.* Academic Press, 489 pp.

Barnes, E. A., and D. L. Hartmann, 2010: Dynamical feedbacks of the southern annular mode in winter and summer. *J. Atmos. Sci.,* **67,** 2320–2330.

Cordron, F., 2007: Relations between annular modes and the mean state: Southern Hemisphere winter. *J. Atmos. Sci.,* **64,** 3328–3339.

Dee, D. P., and Coauthors, 2011: The ERA-Interim reanalysis: Configuration and performance of the data assimilation system. *Quart. J. Roy. Meteor. Soc.,* **137,** 553–597, doi:10.1002/qj.828.

Feldstein, S. B., and S. Lee, 1998: Is the atmospheric zonal index driven by an eddy feedback? *J. Atmos. Sci.,* **55,** 3077–3086.

Hartmann, D. L., and F. Lo, 1998: Wave-driven zonal flow vacillation in the Southern Hemisphere. *J. Atmos. Sci.,* **55,** 1303–1315.

Karoly, D. J., 1990: The role of transient eddies in low-frequency zonal variations of the Southern Hemisphere circulation. *Tellus,* **42A,** 41–50.

Kidson, J. W., 1988: Interannual variations in the Southern Hemisphere circulation. *J. Climate,* **1,** 1177–1198.

Kushner, P. J., I. M. Held, and T. L. Delworth, 2001: Southern Hemisphere atmospheric circulation response to global warming. *J. Climate,* **14,** 2238–2249.

Lau, N.-C., 1988: Variability of the observed midlatitude storm tracks in relation to low-frequency changes in the circulation pattern. *J. Atmos. Sci.,* **45,** 2718–2743.

Limpasuvan, V., and D. L. Hartmann, 2000: Wave-maintained annular modes of climate variability. *J. Climate,* **13,** 4414–4429.

Lorenz, D. J., and D. L. Hartmann, 2001: Eddy–zonal flow feedback in the Southern Hemisphere. *J. Atmos. Sci.,* **58,** 3312–3327.

Lorenz, E. N., 1955: Available potential energy and the maintenance of the general circulation. *Tellus,* **7,** 157–167.

Miller, R. L., G. A. Schmidt, and D. T. Shindell, 2006: Forced annular variations in the 20th century Intergovernmental Panel on Climate Change Fourth Assessment Report models. *J. Geophys. Res.,* **111,** D18101, doi:10.1029/2005JD006323.

North, G. R., T. L. Bell, R. F. Cahalan, and F. J. Moeng, 1982: Sampling errors in the estimation of empirical orthogonal functions. *Mon. Wea. Rev.,* **110,** 699–706.

O'Gorman, P. A., 2010: Understanding the varied response of the extratropical storm tracks to climate change. *Proc. Natl. Acad. Sci. USA,* **107,** 19 176–19 180.

Pfeffer, R. L., 1992: A study of eddy-induced fluctuations of the zonal-mean wind using conventional and transformed Eulerian diagnostics. *J. Atmos. Sci.,* **49,** 1036–1050.

Randel, W. J., and J. L. Stanford, 1985: An observational study of medium-scale wave dynamics in the Southern Hemisphere summer. Part I: Wave structure and energetics. *J. Atmos. Sci.,* **42,** 1172–1188.

Robinson, W. A., 2000: A baroclinic mechanism for the eddy feedback on the zonal index. *J. Atmos. Sci.,* **57,** 415–422.

Simmons, A. J., and B. J. Hoskins, 1978: The life cycles of some nonlinear baroclinic waves. *J. Atmos. Sci.,* **35,** 414–432.

Thompson, D. W. J., and J. M. Wallace, 2000: Annular modes in the extratropical circulation. Part I: Month-to-month variability. *J. Climate,* **13,** 1000–1016.

——, and E. A. Barnes, 2014: Periodic variability in the large-scale Southern Hemisphere atmospheric circulation. *Science,* **343,** 641–645.

Vallis, G. K., 2006: *Atmospheric and Oceanic Fluid Dynamics.* Cambridge University Press, 745 pp.

Webster, P. J., and J. L. Keller, 1974: A strong long-period tropospheric and stratospheric rhythm in the Southern Hemisphere. *Nature,* **248,** 212–213.

——, and ——, 1975: Atmospheric variations: Vacillation and index cycles. *J. Atmos. Sci.,* **32,** 1283–1300.

Wettstein, J. J., and J. M. Wallace, 2010: Observed patterns of month-to-month storm track variability and their relationship to the background flow. *J. Atmos. Sci.,* **67,** 1420–1437.

Yin, J. H., 2005: A consistent poleward shift of the storm tracks in simulations of 21st century climate. *Geophys. Res. Lett.,* **32,** L18701, doi:10.1029/2005GL023684.